

# General First-Principles Approach to Crystals in Finite Magnetic Fields

Chengye Lü<sup>1†</sup>, Yingwei Chen<sup>1†</sup>, Yuzhi Wang<sup>2,3</sup>, Zhihao Dai<sup>1</sup>, Zhong Fang<sup>2,3</sup>, Xin-Gao Gong<sup>1</sup>,  
Quansheng Wu<sup>2,3\*</sup>, Hongjun Xiang<sup>1\*</sup>

<sup>1</sup>*Key Laboratory of Computational Physical Sciences (Ministry of Education), Institute of Computational Physical Sciences, State Key Laboratory of Surface Physics, and Department of Physics, Fudan University, Shanghai, 200433, China*

<sup>2</sup>*Beijing National Laboratory for Condensed Matter Physics and Institute of Physics, Chinese Academy of Sciences, Beijing 100190, China*

<sup>3</sup>*University of Chinese Academy of Sciences, Beijing 100049, China*

\*E-mail: [quansheng.wu@iphy.ac.cn](mailto:quansheng.wu@iphy.ac.cn)

\*E-mail: [hxiang@fudan.edu.cn](mailto:hxiang@fudan.edu.cn)

† These authors contributed equally to this work.

## ABSTRACT

We introduce a general first-principles methodology for computing electronic structure in a finite uniform magnetic field which allows for an arbitrary rational magnetic flux and nonlocal pseudopotentials, at a comparable time complexity of conventional plane-wave pseudopotential approaches in zero-field conditions. The versatility of this method is demonstrated through comprehensive applications to both molecular and crystalline systems, including calculations of magnetizabilities, magnetically induced currents, and magnetic energy bands. Furthermore, we provide rigorous proofs of two fundamental properties for crystals in uniform magnetic fields: the “strong translational symmetry” and “magnetic bands shift” phenomena.

## Introduction

Due to its theoretical and practical significance, the behavior of matter under external electromagnetic fields has attracted increasing attention over the past few decades. Unlike electric fields, magnetic fields uniquely couple with two distinct degrees of freedom (DOF) of charged particles: spin DOF and orbital DOF, each acting like a separate field. The field coupling with the former, often referred to as the spin-Zeeman field, is well-known for primarily governing magnetism, while the field coupling with the latter, which is exclusively termed the “magnetic field” in this Letter, is less familiar but gives rise to a variety of novel phenomena, including the Landau Level [1], the Abrikosov vortex [2], the Quantum Hall Effect (QHE) [3,4], the Fractional Quantum Hall Effect (FQHE) [5], strong-magnetic-field-induced phase transitions [6], fragile topology [7,8], among others.

First-principles calculations using Kohn-Sham Density Functional Theory (KS-DFT) [9,10] are fundamental tools for investigating material properties in condensed matter physics and material science. While significant advancements have been made in developing DFT methods for systems under finite electric fields [11,12] and spin-Zeeman fields [13,14], progress in extending DFT to finite magnetic fields has remained relatively slow. Although recent efforts utilizing London orbitals have improved the treatment of molecular systems in magnetic fields [15–18], the development of such methods for crystalline systems is still in its early stages, posing significant challenges for accurately capturing magnetic-field-induced electronic structure effects. The primary challenge in applying a finite magnetic field to periodic systems is that the field breaks the original Bloch translational symmetry under the periodic boundary conditions (PBC),

rendering the commonly used plane-wave (PW) basis set unsuitable. Thus, previous studies commonly use the perturbation theory to incorporate magnetic fields into DFT computations [19,20], but these approaches cannot simulate phenomena associated with magnetic fields beyond the perturbative regime, such as the Landau Level and QHE, as previously mentioned, much less exotic physics in extremely strong fields on white dwarfs and neutron stars [21].

In 2004, Cai *et al.* proposed a novel *ab initio* approach for periodic systems under a finite uniform magnetic field, by introducing a so-called “plane-wave-like” basis set which aligns with the magnetic periodic boundary conditions (MPBC) and the magnetic translational symmetry (MTS), to diagonalize the finite-field Hamiltonian [22,23]. However, their approach has limitations: first, their magnetic flux number is not arbitrary but constrained to being a factor of the number of discrete grid-points along the  $y$ -direction; second, they cannot treat Hamiltonians with nonlocal pseudopotentials which are however indispensable for treating most elements. To integrate nonlocal pseudopotentials into field-containing computations, Pickard *et al.* proposed the gauge-including projector augmented-wave (GIPAW) method [24,25]. This method has been proven effective for computations in the perturbative regime of an external magnetic field [24–28], but hasn’t been extended to the finite-field regime yet.

In this Letter, we present a general finite-field first-principles approach for periodic systems that accommodates arbitrary rational magnetic fluxes and Hamiltonians with or without nonlocal pseudopotentials, through combining the fast Fourier transform (FFT) and real-space algorithms. We present applications of this novel method to both molecular and crystal systems by computing magnetizabilities, magnetically induced currents and magnetic energy bands. The whole algorithm is implemented in a developer’s version of the Property Analysis and Simulation Package for materials (PASP) [29].

## Methods

**Hamiltonian and wavefunction-**We adopt the atomic unit system ( $\hbar = e = m_e = 1$ ) throughout this Letter, where  $\hbar$  is the reduced Planck constant,  $e$  is the elementary charge and  $m_e$  is the electron mass. Consider a spin-less crystalline system with lattice periodicities  $\mathbf{a}_\alpha$  ( $\alpha = 1, 2, 3$ ), the KS Hamiltonian for the system, which employs Kleinman-Bylander pseudopotentials [30], in the presence of a uniform magnetic field  $\mathbf{B}$  is written as

$$\hat{H} := \frac{1}{2} \hat{\pi}^2 + V_{\text{per}}(\mathbf{r}) + \hat{V}_{\text{GIPAW}}, \quad (1)$$

where  $\hat{\pi} := -i\nabla + \mathbf{A}(\mathbf{r})$  is the mechanical momentum operator and  $\mathbf{A}(\mathbf{r})$  is the magnetic vector potential satisfying the condition  $\nabla \times \mathbf{A} = \mathbf{B}$  and the linearity  $\mathbf{A}(\mathbf{r}_1 + \mathbf{r}_2) = \mathbf{A}(\mathbf{r}_1) + \mathbf{A}(\mathbf{r}_2)$ . The periodic local potential  $V_{\text{per}}(\mathbf{r})$ , defined by  $V_{\text{per}}(\mathbf{r}) = V_{\text{per}}(\mathbf{r} + \mathbf{a}_\alpha)$  with  $\mathbf{a}$  as the lattice vector, consists of three terms: the local pseudopotential  $V_{\text{loc}}(\mathbf{r})$ , the Hartree potential  $V_{\text{H}}[\rho](\mathbf{r})$  and the exchange-correlation potential  $V_{\text{xc}}[\rho](\mathbf{r})$ , where  $\rho$  denotes the electronic density. Here we neglect the dependence of exchange-correlation functional on the magnetic-field or current, and a detailed discussion of density functional approximations in a magnetic field is beyond the scope of this work [31–36]. The final term  $\hat{V}_{\text{GIPAW}}$  (to be discussed below) represents the non-local contribution from the GIPAW method [24,25] which ensures the recovery of MTS.

As discovered in previous studies, when the magnetic field satisfies the magnetic flux quantization condition, i.e.,  $\mathbf{B} \cdot (\mathbf{a}_1 \times \mathbf{a}_2) = 2\pi n_\Phi$  where  $n_\Phi \in \mathbb{Z}$  is the magnetic flux number, the eigenstates  $\{\psi_{ik}\}$  of the Hamiltonian, corresponding to the eigenvalues  $\{\epsilon_{ik}\}$ , obey the magnetic Bloch theorem (MBT) [22,23,37–41]

$$\psi_{ik}(\mathbf{r}) = e^{i\mathbf{k} \cdot \mathbf{r}} u_{ik}(\mathbf{r}), \quad (2.1)$$

$$u_{ik}(\mathbf{r} + \mathbf{a}_\alpha) = e^{-i\mathbf{A}(\mathbf{a}_\alpha) \cdot \mathbf{r}} u_{ik}(\mathbf{r}), \quad (2.2)$$

where  $i$  denotes the band index and  $\mathbf{k}$  belongs to the first Brillouin Zone (FBZ). Our task is to solve the KS Hamiltonian (1) under the MPBC described by equations (2.2) through the self-consistency-field (SCF) loop. It is important to note that the theorem can be generalized to any rational values of  $n_\Phi = p/q$  with  $p$  and  $q$  coprime since it's always possible to enlarge the unit cell by a factor of  $q$  to construct a magnetic unit cell that quantizes the magnetic flux. Hereafter, unless specially stated, we do not distinguish between the magnetic unit cell and the (chemical) unit cell, or between the magnetic Brillouin zone and the Brillouin zone. Moreover, it's also helpful to note that the electronic density  $\rho(\mathbf{r})$  and the physical current density  $\mathbf{j}(\mathbf{r})$  generated by magnetic Bloch functions are periodic with respect to the magnetic unit cell:

$$\rho(\mathbf{r}) := \sum_{ik} f_{ik} |\psi_{ik}(\mathbf{r})|^2 = \rho(\mathbf{r} + \mathbf{a}_\alpha), \quad (3.1)$$

$$\mathbf{j}(\mathbf{r}) := - \sum_{ik} f_{ik} \Re[\psi_{ik}^*(\mathbf{r}) \hat{\pi} \psi_{ik}(\mathbf{r})] = \mathbf{j}(\mathbf{r} + \mathbf{a}_\alpha), \quad (3.2)$$

where  $f_{ik}$  denotes the occupation number and  $\Re$  represents the real part. Remarkably, one can prove that both  $\rho(\mathbf{r})$  and  $\mathbf{j}(\mathbf{r})$  are periodic not only within the magnetic unit cell but also within

the (chemical) unit cell. This theorem, which we refer to as “strong translational symmetry”, is proven in the supplementary materials [42].

In our approach, we assume that the magnetic field is oriented along the  $\mathbf{a}_3$  direction, i.e.,  $\mathbf{B} = B\hat{\mathbf{a}}_3 = 2\pi n_\Phi \mathbf{a}_3 / \Omega$ , and we adopt the Landau gauge [23,43,44] defined by  $\mathbf{A}_{\text{Lan}}(\mathbf{r}) := 2\pi n_\Phi (\mathbf{b}^1 \cdot \mathbf{r}) \mathbf{b}^2$ , where  $\hat{\mathbf{a}}_3$  is the unit vector of  $\mathbf{a}_3$ -direction,  $\Omega := \mathbf{a}_3 \cdot (\mathbf{a}_1 \times \mathbf{a}_2)$  is the volume of the unit cell and  $\mathbf{b}^\alpha$  ( $\alpha = 1, 2, 3$ ) are the (scaled) reciprocal basis vectors defined by  $\mathbf{b}^\alpha \cdot \mathbf{a}_\beta = \delta_\beta^\alpha$  for  $\alpha, \beta = 1, 2, 3$ . Under this gauge, the MPBC is explicitly written as

$$\begin{aligned} u_{ik}(\xi^1 + 1, \xi^2, \xi^3) &= e^{-i2\pi n_\Phi \xi^2} u_{ik}(\xi^1, \xi^2, \xi^3), \\ u_{ik}(\xi^1, \xi^2 + 1, \xi^3) &= u_{ik}(\xi^1, \xi^2, \xi^3 + 1) = u_{ik}(\xi^1, \xi^2, \xi^3), \end{aligned} \quad (4)$$

where  $\mathbf{r} = \sum_{\alpha=1}^3 \xi^\alpha \mathbf{a}_\alpha$ , with  $\xi^\alpha \in [0, 1)$ . Our method can, in principle, be generalized to any gauge. Since the local potential in Eq. (1) acts as a direct multiplication in real-space, we focus on the algorithms for the kinetic and nonlocal terms in the following paragraphs.

**Algorithm on kinetic operator**-In field-free DFT, the kinetic term is represented by a three-dimensional Laplacian and can be efficiently implemented using the FFT technique compatible with PBC. When a magnetic field is applied, the kinetic term involves the vector potential, and the MPBC in Eq. (4) introduces non-periodicity along the  $\mathbf{a}_1$  direction. Interestingly, similar FFT-based techniques can still be utilized by introducing a set of auxiliary functions [45] defined as  $h_{ik}^{n_\Phi}(\xi^1, \xi^2, \xi^3) := \exp(i2\pi n_\Phi \xi^1 \xi^2) u_{ik}(\xi^1, \xi^2, \xi^3)$ , which are periodic along  $\mathbf{a}_1$  and  $\mathbf{a}_3$  but non-periodic along  $\mathbf{a}_2$ . To formulate the algorithm, we rewrite the kinetic operator as  $\frac{1}{2} \sum_{\alpha\beta} g^{\alpha\beta} \hat{\pi}_\alpha \hat{\pi}_\beta$ , where  $\hat{\pi}_\alpha := \mathbf{a}_\alpha \cdot \hat{\boldsymbol{\pi}} = -i\partial/\partial\xi^\alpha + A_\alpha$  and  $A_\alpha := \mathbf{a}_\alpha \cdot \mathbf{A}$  represent the covariant components of the kinetic momentum and vector potential respectively, and  $g^{\alpha\beta} := \mathbf{b}^\alpha \cdot \mathbf{b}^\beta$  represents the contravariant metric tensor. To be more specific: for  $\hat{\pi}_2$  and  $\hat{\pi}_3$ , the derivatives  $\partial/\partial\xi^\alpha$  and vector potentials  $A_\alpha$  are computed through standard FFT and direct multiplication in real-space, respectively; for  $\hat{\pi}_1 = -i\partial/\partial\xi^1$ , we use the relation that

$$\hat{\pi}_1 u_{ik} = -2\pi n_\Phi \xi^2 u_{ik} + e^{-i2\pi n_\Phi \xi^1 \xi^2} \left( -i \frac{\partial}{\partial \xi^1} h_{ik}^{n_\Phi} \right), \quad (5)$$

where the first term can be computed via real-space multiplication and the second term via FFT due to the  $\xi^1$ -periodicity of  $h_{ik}^{n_\Phi}$ . Thus, the entire kinetic term can be efficiently computed by applying these methods step by step.

**Algorithm on nonlocal pseudopotentials**-The nonlocal term by the GIPAW formulation

writes as  $\hat{V}_{\text{GIPAW}} := \sum_{\mathbf{R},n} |\tilde{p}_{\mathbf{R},n}\rangle a_n^{\mathbf{R}} \langle \tilde{p}_{\mathbf{R},n}|$  with  $\{a_n^{\mathbf{R}}\}$  the nonlocal strength on each atomic site  $\mathbf{R}$  and each channel  $n$ , and the corresponding nonlocal projectors  $\{\tilde{p}_{\mathbf{R},n}\}$  defined as

$$\tilde{p}_{\mathbf{R},n}(\mathbf{r}) := \exp[-i\mathbf{A}_{\text{Lan}}(\mathbf{R}) \cdot \mathbf{r} - if(\mathbf{r} - \mathbf{R})] p_{\mathbf{R},n}(\mathbf{r}), \quad (6)$$

where  $\{p_{\mathbf{R},n}\}$  represents the nonlocal pseudopotential projectors without magnetic fields. The first phase factor,  $\exp[-i\mathbf{A}_{\text{Lan}}(\mathbf{R}) \cdot \mathbf{r}]$ , in Eq. (6) properly restores the MTS of nonlocal pseudopotentials under the magnetic field [24,25]. The second phase factor,  $\exp[-if(\mathbf{r} - \mathbf{R})]$ , where  $\nabla f(\mathbf{r}) := \mathbf{A}_{\text{Lan}}(\mathbf{r}) - \mathbf{A}_{\text{sym}}(\mathbf{r})$  denotes the gauge transformation between the symmetric and Landau gauge, introduces an extra phase when using a non-symmetric gauge, such as the Landau gauge in our approach. Inclusion of this second phase factor is essential because field-free orbitals (or projectors) can only approximate magnetic orbitals (or projectors) under the symmetric gauge  $\mathbf{A}_{\text{sym}}(\mathbf{r}) := \mathbf{B} \times \mathbf{r}/2$  owing to symmetry considerations, as noted in Ref. [39]. Moreover, since we only employ norm-conserving pseudopotentials [46,47] in this work, the GIPAW correction to the non-local strength  $a_n^{\mathbf{R}}$  can be safely omitted [24]. We follow the conventional real-space implementation of nonlocal pseudopotentials [48,49] in our approach, with the key distinction that nonlocal projectors incorporate additional phases as defined in Eq. (6). Specifically, each projector value for each atomic site, together with its corresponding gauge-dependent phases, is precomputed and stored on every real-space grid point within the projector's cutoff radius via interpolation. These projectors are subsequently applied to the wavefunction during the DFT calculation.

## Results

**Test on molecules-**We begin by validating our method via calculating the magnetic susceptibilities, or magnetizabilities, for both closed-shell diamagnetic and closed-shell paramagnetic molecules composed of light elements. Magnetizability is defined as the negative second-order derivative of the total energy with respect to the magnetic field, and can be evaluated using the second-order finite-difference method within our finite-field framework

$$\chi_B := -\frac{\partial^2 E(B)}{\partial B^2} \Big|_{B=0} \approx -\frac{E(\Delta B) - 2E(0) + E(-\Delta B)}{\Delta B^2}, \quad (7)$$

where  $\Delta B$  denotes the magnetic field in the supercell at  $n_{\Phi} = 1$  ( $\approx 2871$  T). We ensure  $E(\Delta B)$  equals to  $E(-\Delta B)$  within numerical accuracy in our computations. Note that, in principle, only the magnetizability contributed by valence electrons can be computed via the pseudopotential

approximation, while for elements lighter than neon the core contributions can be neglected [19]. The computed magnetizabilities are listed in the Table 1, where all DFT calculations are performed at the generalized gradient approximation (GGA) level using PBE functional [50] with energy cut-off of 60 Hartree in a cubic supercell of size  $12\text{\AA} \times 12\text{\AA} \times 12\text{\AA}$ . The molecular configurations and comparative results at finite-field HF and Coupled-Cluster-Single-Double (CCSD) levels using London orbitals are extracted from Ref. [34]. Our approach gives comparable results to all molecules we consider.

To further validate our finite-field DFT method in the molecular level, we calculate the magnetically induced current density of benzene perpendicular to the magnetic field, known as ring currents [51], as plotted in Fig. 1 (a). The calculation is performed with energy cut-off of 20 Hartree in a cuboid supercell of size  $12\text{\AA} \times 12\text{\AA} \times 9\text{\AA}$  with  $n_\Phi = 1$ . We observe a primary diamagnetic vortex flowing around the molecule’s tails, small diamagnetic vortexes surrounding the C-H and C-C bonds and a paramagnetic vortex rotating in the opposite direction at the center. Our results generally agree well with those in Ref. [52] which used London orbitals. The discrepancy near the carbon nuclei should be attributed to our neglect of core electrons.

	PBE-DFT	HF	CCSD
Be	-225.7	-227.8	-214.0
H <sub>2</sub>	-72.5	-69.2	-68.4
CO	-299.0	-299.8	-300.0
HF	-175.4	-175.5	-178.5
H <sub>2</sub> O	-238.6	-232.9	-235.4
AlH	246.0	277.3	233.5
BH	510.3	560.2	411.2

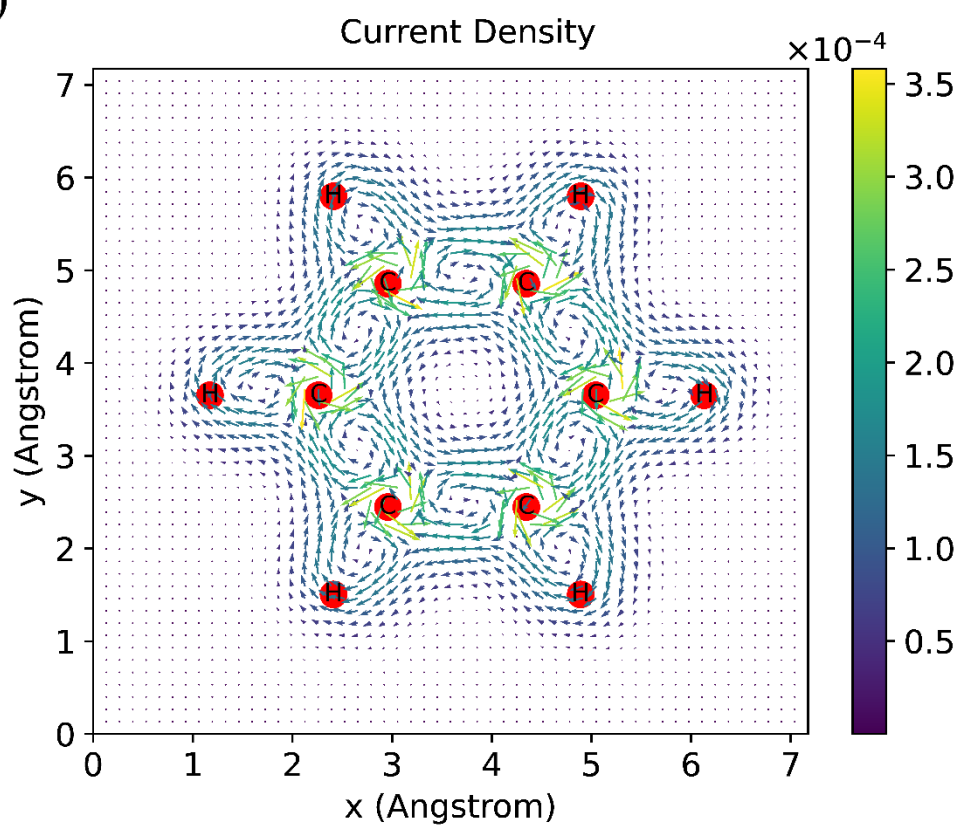
Table 1. Molecular magnetizabilities calculated at the PBE-DFT, HF and CCSD levels of theory in units of  $10^{-30} \text{ J T}^{-2}$ . PBE-DFT results are obtained by our finite-field approach while HF and CCSD results are extracted from Ref. [34] in which London orbitals are used.

For all diamagnetic molecules we have computed, we observe an increase not only in the total energy but also in the absolute values of both kinetic energy and local potential energy, indicating the induced precession and localization of electrons by the external magnetic field [34,53]. To visualize this phenomenon, we plot the density variation of benzene after and before the

application of the field, as shown in Fig. 1 (b). For (closed-shell) paramagnetic molecules, in contrast, both the total energy and the absolute values of kinetic energy and local potential energy decrease when subjected to a magnetic field.



(a)



(b)

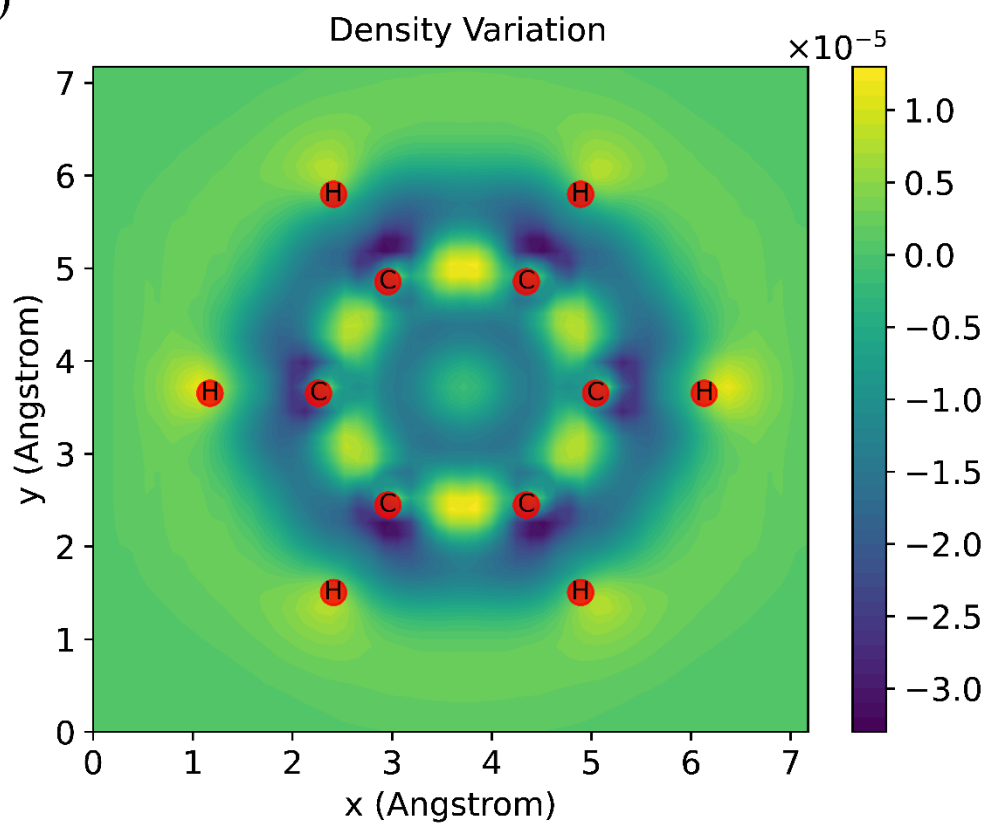


FIG. 1. Benzene molecule in a uniform magnetic field of approximately 2871 T. (a) Magnetically induced current density of valence electrons. (b) Electron density variation under the applied magnetic field.

**Test on solids**-Similar to the molecular test, we first compute the (valence) magnetizabilities for solids including inert-gas crystals and semiconductors, with the results presented in Table 2. All DFT calculations are performed within the local density approximation (LDA) [54]. For argon and krypton solids at FCC phases, calculations are carried out on a  $6 \times 6 \times 6$  Monkhorst-Pack  $\mathbf{k}$ -point grid [55] with an energy-cutoff of 40 Hartree. For semiconductors, namely diamond ( $\text{C}_2$ ) and silicon ( $\text{Si}_2$ ), we expand the conventional FCC cell along the direction of  $\mathbf{a}_1$  by a factor of three to reduce the magnetic strength, and then perform calculations on a  $2 \times 6 \times 6$   $\mathbf{k}$ -point grid with energy-cutoffs of 40 and 20 Hartree, respectively. The core contribution to the magnetizabilities, valence contribution computed via all-electron perturbation theory at the LDA level, and experimental data are all extracted from Ref. [19]. Our finite-field approach yields magnetizabilities for argon and krypton comparable to those via the all-electron perturbative method. For diamond and silicon, our finite field results agree better with the experimental values than the previous results from the perturbative method. In particular,  $\chi^{\text{finite field}}$ ,  $\chi^{\text{perturb}}$ ,  $\chi^{\text{expt}}$  for silicon are -5.0, -1.2, -6.4 (in units of  $10^{-6} \text{ cm}^3/\text{mole}$ ), respectively.

	Lattice constant ( $\text{\AA}$ )	$\chi_{\text{core}}$	$\chi_{\text{val}}^{\text{finite field}}$	$\chi_{\text{val}}^{\text{perturb}}$	$\chi^{\text{finite field}}$	$\chi^{\text{perturb}}$	$\chi^{\text{expt}}$
Ar	5.36	-1.19	-19.2	-19.97	-20.39	-20.84	-
Kr	5.79	-5.41	-24.6	-24.90	-30.01	-30.31	-
diamond	3.56	-0.3	-11.2	-10.3	-11.5	-10.6	-11.8
silicon	5.44	-4.8	-0.2	3.6	-5.0	-1.2	-6.4

Table 2. Solid-state magnetizabilities computed via finite-field and perturbative approaches within LDA-DFT in units of  $10^{-6} \text{ cm}^3/\text{mole}$ . The core and valence contributions obtained via all-electron perturbation theory, along with the experimental results, are extracted from Ref. [19].

Subsequently, we compute the magnetic band structure of the solid. To highlight the magnetic influence, we present the band structures of graphene computed through the PBE functional with energy cutoffs of 40 Hartree, both before and after the application of a magnetic field of  $n_{\Phi} =$

1 (approximately 80125 T) in Fig. 2(a) and 2(b), respectively. These bands are obtained from non-SCF calculations based on charge densities obtained from field-free and field-containing SCF calculations, respectively. It is evident from these figures that the energy bands are significantly changed and flattened under the strong magnetic field. Furthermore, we attribute these alterations primarily to the modifications in the Hamiltonian and boundary conditions resulting from the incorporation of the magnetic flux, rather than to variations in the density induced by the magnetic field, which remains negligible even at such a high field strength. To substantiate this assertion, we compare the magnetic bands shown in Fig. 2(b) with those in Fig. 2(c), which are computed at the same field strength but with the electronic density fixed to the field-free case, the same one as in Fig. 2(a). The minor discrepancies observed between these two band structures as well as total energies support our claim that the changes are predominantly flux-driven.

However, we find that the magnetic bands are not invariant with respect to a collective atomic translation of the structure, different from the field-free case. As shown in Fig. 2(d), we display the magnetic bands at the same field strength after applying a collective atomic translation of  $0.5 \mathbf{a}_1$ . Remarkably, these bands deviate significantly from those in Fig. 2(b), revealing that the magnetic band structure  $\{\epsilon_{i\mathbf{k}} | \mathbf{k} \in \text{FBZ}\}$  lacks translational invariance in contrast to the field-free scenario. This phenomenon, referred to as “magnetic band shift” in this Letter, arises because the atomic translation modifies only the scalar potential in the Hamiltonian. But this modification is mathematically equivalent to a linear gauge transformation of the vector potential, which introduces an additional position-dependent phase to the eigenstates. The phase can then be absorbed into a redefinition of  $\mathbf{k}$ -points within the FBZ, leading to a shift of the energy levels onto new  $\mathbf{k}$ -points. That is, the band structure undergoes an overall shift due to the atomic movement. Consequently, the absolute shape of the magnetic bands loses physical significance, and its interpretation becomes ambiguous. Nevertheless, the density of states (DOS) as well as the total energy remains translationally invariant, as illustrated in Fig. 2(e) and 2(f), strengthening our argument. Details and additional examples of “magnetic band shift” are provided in the supplementary material [42].

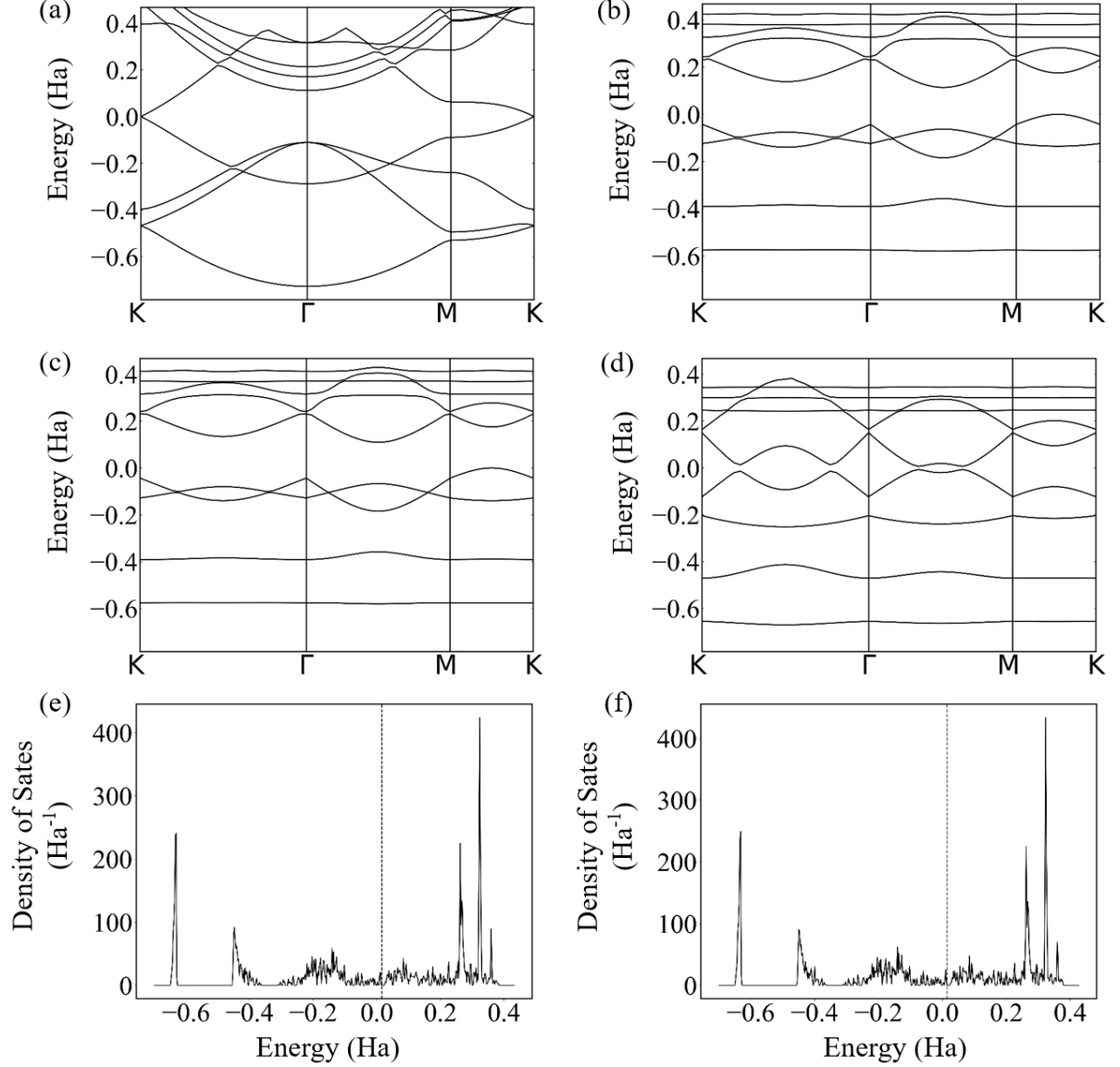


FIG. 2. Magnetic field effects on the band structure of graphene. (a) Electronic band structure in the absence of an external magnetic field. (b) Magnetic band structure under an external magnetic field of  $n_\phi = 1$  (approximately 80125 T). (c) Magnetic band structure under the same field strength as in (b), but using the electron density from the field-free SCF calculation shown in (a). (d) Magnetic band structure under the same field strength as in (b), following a collective atomic translation of  $0.5 \mathbf{a}_1$ . (e), (f) Density of states (DOS) of graphene under the same magnetic field as in (b), before and after the collective atomic translation of  $0.5 \mathbf{a}_1$ , respectively. The red dotted line indicates the Fermi energy.

Finally, we compute the Berry curvatures and Chern numbers of graphene under a magnetic field of  $n_\Phi = 1$ , using Fukui's algorithm [56,57]. Although the topologically non-trivial nature of magnetic bands, characterized by non-zero Chern numbers, has been established through earlier mathematical analyses [4,58], it has not yet been verified from a first-principles perspective. As a preliminary validation, we disable all scalar potentials in the Hamiltonian to solve the famous Landau problem and, as a result, successfully recover the equally spaced flat bands with a constant Berry curvature of magnitude  $1/B$ , whose integration over the FBZ yields a Chern number of 1 [59]. We then apply this procedure to graphene, whose lowest valence band exhibits a non-constant Berry curvature but still yields a Chern number of 1, thereby confirming the non-trivial topology of magnetic bands. Moreover, the second lowest band yields a Chern number of 0 while the entangled third and fourth lowest bands yield a Chern number of 3 jointly, indicating magnetic bands cannot be naively interpreted as Landau Levels in general. All computations in this paragraph are implemented using the PBE functional with an energy cutoff of 30 Hartree and a  $\mathbf{k}$ -point grid of size  $40 \times 40 \times 1$ . For illustration, the Berry curvatures of the two lowest bands of graphene are presented in Fig. 3.

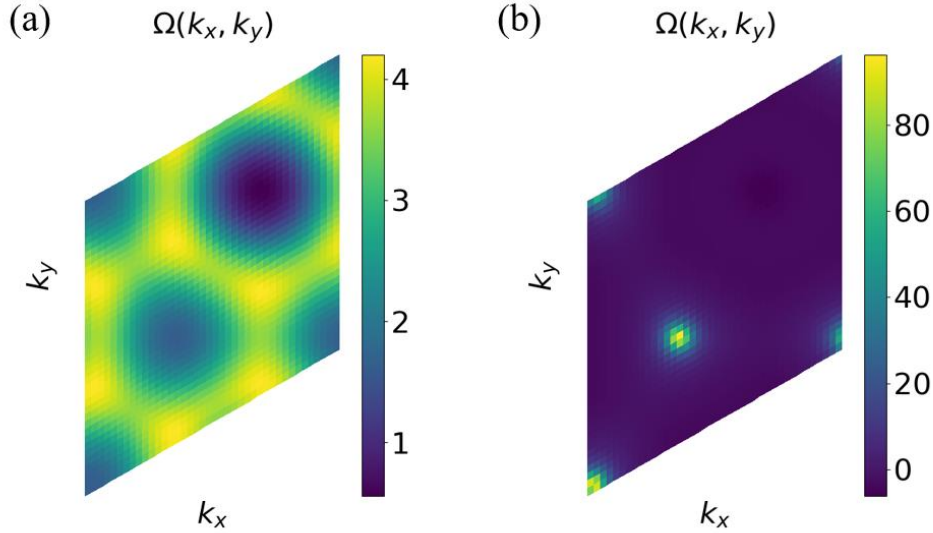


FIG. 3. Berry curvature distributions in graphene under a magnetic field of  $n_\Phi = 1$  (approximately 80125 T). (a) Berry curvature of the lowest energy band, which carries a Chern number of 1. (b) Berry curvature of the second lowest energy band, which has a Chern number of 0.

## **Conclusion**

In summary, we have presented a new first-principles scheme for computing the electronic structure of crystals in uniform magnetic fields of an arbitrary rational quantum flux. The algorithm combines FFT technique and real-space methods, at a computational time complexity to that of conventional field-free DFT based on PW basis and pseudopotential approximations. This algorithm is also the first application of the GIPAW method in finite-field regimes. The computation of ionic forces, as well as extensions of this method to incorporate other variables like spin-density, current density and spin-current density [60], is straightforward and will be investigated in our future works.

## **Acknowledgement**

We acknowledge financial support from NSFC (No. 12188101), the National Key R&D Program of China (No. 2022YFA1402901, 2023YFA1607400), the Guangdong Major Project of the Basic and Applied Basic Research (Future functional materials under extreme conditions—2021B0301030005), Shanghai Science and Technology Program (No. 23JC1400900), and Shanghai Pilot Program for Basic Research—FuDan University 21TQ1400100 (23TQ017), New Cornerstone Science Foundation. We thank Prof. Wei Hu for discussions about DFT and thank Tao Zhang for discussions about quantum mechanics.

## References

- [1] L. D. Landau and E. M. Lifshitz, *Quantum Mechanics: Non-Relativistic Theory* (Elsevier, 1981).
- [2] A. A. Abrikosov, Nobel Lecture: Type-II superconductors and the vortex lattice, *Rev. Mod. Phys.* **76**, 975 (2004).
- [3] K. v. Klitzing, G. Dorda, and M. Pepper, New Method for High-Accuracy Determination of the Fine-Structure Constant Based on Quantized Hall Resistance, *Phys. Rev. Lett.* **45**, 494 (1980).
- [4] D. J. Thouless, M. Kohmoto, M. P. Nightingale, and M. den Nijs, Quantized Hall Conductance in a Two-Dimensional Periodic Potential, *Phys. Rev. Lett.* **49**, 405 (1982).
- [5] D. C. Tsui, H. L. Stormer, and A. C. Gossard, Two-Dimensional Magnetotransport in the Extreme Quantum Limit, *Phys. Rev. Lett.* **48**, 1559 (1982).
- [6] K. Higuchi, D. B. Hamal, and M. Higuchi, Second-order phase transition of silicon from a band insulator to metal induced by strong magnetic fields, *New J. Phys.* **24**, 103028 (2022).
- [7] B. Lian, F. Xie, and B. A. Bernevig, Landau level of fragile topology, *Phys. Rev. B* **102**, 041402 (2020).
- [8] J. Herzog-Arbeitman, Z.-D. Song, N. Regnault, and B. A. Bernevig, Hofstadter Topology: Noncrystalline Topological Materials at High Flux, *Phys. Rev. Lett.* **125**, 236804 (2020).
- [9] P. Hohenberg and W. Kohn, Inhomogeneous Electron Gas, *Phys. Rev.* **136**, B864 (1964).
- [10] W. Kohn and L. J. Sham, Self-Consistent Equations Including Exchange and Correlation Effects, *Phys. Rev.* **140**, A1133 (1965).
- [11] I. Souza, J. Íñiguez, and D. Vanderbilt, First-Principles Approach to Insulators in Finite Electric Fields, *Phys. Rev. Lett.* **89**, 117602 (2002).
- [12] J. W. Zwanziger, J. Galbraith, Y. Kipouros, M. Torrent, M. Giantomassi, and X. Gonze, Finite homogeneous electric fields in the projector augmented wave formalism: Applications to linear and nonlinear response, *Comput. Mater. Sci.* **58**, 113 (2012).
- [13] U. V. Barth and L. Hedin, A local exchange-correlation potential for the spin polarized case. i, *J. Phys. C Solid State Phys.* **5**, 1629 (1972).
- [14] E. Bousquet, N. A. Spaldin, and K. T. Delaney, Unexpectedly Large Electronic Contribution to Linear Magnetoelectricity, *Phys. Rev. Lett.* **106**, 107202 (2011).
- [15] E. I. Tellgren, T. Helgaker, and A. Soncini, Non-perturbative magnetic phenomena in closed-shell paramagnetic molecules, *Phys. Chem. Chem. Phys.* **11**, 5489 (2009).
- [16] E. I. Tellgren, A. M. Teale, J. W. Furness, K. K. Lange, U. Ekström, and T. Helgaker, Non-perturbative calculation of molecular magnetic properties within current-density functional theory, *J. Chem. Phys.* **140**, 034101 (2014).
- [17] D. B. Williams-Young et al., The Chronus Quantum software package, *WIREs Comput. Mol. Sci.* **10**, e1436 (2020).
- [18] Y. J. Franzke et al., TURBOMOLE: Today and Tomorrow, *J. Chem. Theory Comput.* **19**, 6859 (2023).
- [19] K. Ohno, F. Mauri, and S. G. Louie, Magnetic susceptibility of semiconductors by an all-electron first-

principles approach, Phys. Rev. B **56**, 1009 (1997).

[20] F. Mauri and S. G. Louie, Magnetic susceptibility of insulators from first principles, Phys. Rev. Lett. **76**, 4246 (1996).

[21] H. Ruder, G. Wunner, H. Herold, and F. Geyer, *Atoms in Strong Magnetic Fields* (Springer, Berlin, Heidelberg, 1994).

[22] W. Cai and G. Galli, *Ab Initio* Calculations in a Uniform Magnetic Field Using Periodic Supercells, Phys. Rev. Lett. **92**, 186402 (2004).

[23] E. Lee, W. Cai, and G. A. Galli, Electronic structure calculations in a uniform magnetic field using periodic supercells, J. Comput. Phys. **226**, 1310 (2007).

[24] C. J. Pickard and F. Mauri, All-electron magnetic response with pseudopotentials: NMR chemical shifts, Phys. Rev. B **63**, 245101 (2001).

[25] J. R. Yates, C. J. Pickard, and F. Mauri, Calculation of NMR chemical shifts for extended systems using ultrasoft pseudopotentials, Phys. Rev. B **76**, 024401 (2007).

[26] C. J. Pickard and F. Mauri, First-Principles Theory of the EPR  $\mathbf{g}$  Tensor in Solids: Defects in Quartz, Phys. Rev. Lett. **88**, 086403 (2002).

[27] D. Ceresoli, U. Gerstmann, A. P. Seitsonen, and F. Mauri, First-principles theory of orbital magnetization, Phys. Rev. B **81**, 060409 (2010).

[28] J. W. Zwanziger, M. Torrent, and X. Gonze, Orbital magnetism and chemical shielding in the projector augmented-wave formalism, Phys. Rev. B **107**, 165157 (2023).

[29] F. Lou, X. Y. Li, J. Y. Ji, H. Y. Yu, J. S. Feng, X. G. Gong, and H. J. Xiang, PASP: Property analysis and simulation package for materials, J. Chem. Phys. **154**, 114103 (2021).

[30] L. Kleinman and D. M. Bylander, Efficacious Form for Model Pseudopotentials, Phys. Rev. Lett. **48**, 1425 (1982).

[31] G. Vignale and M. Rasolt, Density-functional theory in strong magnetic fields, Phys. Rev. Lett. **59**, 2360 (1987).

[32] C. J. Grayce and R. A. Harris, Magnetic-field density-functional theory, Phys. Rev. A **50**, 3089 (1994).

[33] J. W. Furness, J. Verbeke, E. I. Tellgren, S. Stopkiewicz, U. Ekström, T. Helgaker, and A. M. Teale, Current Density Functional Theory Using Meta-Generalized Gradient Exchange-Correlation Functionals, J. Chem. Theory Comput. **11**, 4169 (2015).

[34] S. Reimann, A. Borgoo, J. Austad, E. I. Tellgren, A. M. Teale, T. Helgaker, and S. Stopkiewicz, Kohn-Sham energy decomposition for molecules in a magnetic field, Mol. Phys. **117**, 97 (2019).

[35] S. Lehtola, M. Dimitrova, H. Fliegl, and D. Sundholm, Benchmarking Magnetizabilities with Recent Density Functionals, J. Chem. Theory Comput. **17**, 1457 (2021).

[36] C. J. Schattenberg, A. Wodyński, H. Åström, D. Sundholm, M. Kaupp, and S. Lehtola, Revisiting Gauge-Independent Kinetic Energy Densities in Meta-GGAs and Local Hybrid Calculations of Magnetizabilities, J. Phys. Chem. A **127**, 10896 (2023).

[37] D. Xiao, M.-C. Chang, and Q. Niu, Berry phase effects on electronic properties, Rev. Mod. Phys. **82**, 1959 (2010).

[38] S. Janecek, M. Aichinger, and E. R. Hernández, Two-dimensional Bloch electrons in perpendicular magnetic fields: An exact calculation of the Hofstadter butterfly spectrum, Phys. Rev. B **87**, 235429 (2013).

[39] K. Higuchi, D. B. Hamal, and M. Higuchi, Relativistic tight-binding approximation method for materials immersed in a uniform magnetic field: Application to crystalline silicon, Phys. Rev. B **91**, 075122 (2015).

[40] J. Herzog-Arbeitman, A. Chew, and B. A. Bernevig, Magnetic Bloch theorem and reentrant flat bands in twisted bilayer graphene at  $2\pi$  flux, Phys. Rev. B **106**, 085140 (2022).



- [41] X. Wang and O. Vafek, Revisiting Bloch electrons in a magnetic field: Hofstadter physics via hybrid Wannier states, *Phys. Rev. B* **108**, 245109 (2023).
- [42] Supplementary Material for General First-Principles Approach to Crystals in Uniform Magnetic Fields, (n.d.).
- [43] N. Nemec and G. Cuniberti, Hofstadter butterflies of bilayer graphene, *Phys. Rev. B* **75**, 201404 (2007).
- [44] Y. Fang and J. Cano, Symmetry indicators in commensurate magnetic flux, *Phys. Rev. B* **107**, 245108 (2023).
- [45] E. Onofri, *Landau Levels on the 2D Torus: A Numerical Approach*, arXiv:0804.3673.
- [46] D. R. Hamann, M. Schlüter, and C. Chiang, Norm-Conserving Pseudopotentials, *Phys. Rev. Lett.* **43**, 1494 (1979).
- [47] D. R. Hamann, Optimized norm-conserving Vanderbilt pseudopotentials, *Phys. Rev. B* **88**, 085117 (2013).
- [48] R. D. King-Smith, M. C. Payne, and J. S. Lin, Real-space implementation of nonlocal pseudopotentials for first-principles total-energy calculations, *Phys. Rev. B* **44**, 13063 (1991).
- [49] J.-I. Iwata, D. Takahashi, A. Oshiyama, T. Boku, K. Shiraishi, S. Okada, and K. Yabana, A massively-parallel electronic-structure calculations based on real-space density functional theory, *J. Comput. Phys.* **229**, 2339 (2010).
- [50] J. P. Perdew, K. Burke, and M. Ernzerhof, Generalized Gradient Approximation Made Simple, *Phys. Rev. Lett.* **77**, 3865 (1996).
- [51] P. Lazzeretti, Ring currents, *Prog. Nucl. Magn. Reson. Spectrosc.* **36**, 1 (2000).
- [52] T. J. P. Irons, L. Spence, G. David, B. T. Speake, T. Helgaker, and A. M. Teale, Analyzing Magnetically Induced Currents in Molecular Systems Using Current-Density-Functional Theory, *J. Phys. Chem. A* **124**, 1321 (2020).
- [53] K. K. Lange, E. I. Tellgren, M. R. Hoffmann, and T. Helgaker, A Paramagnetic Bonding Mechanism for Diatomics in Strong Magnetic Fields, *Science* **337**, 327 (2012).
- [54] J. P. Perdew and Y. Wang, Accurate and simple analytic representation of the electron-gas correlation energy, *Phys. Rev. B* **45**, 13244 (1992).
- [55] H. J. Monkhorst and J. D. Pack, Special points for Brillouin-zone integrations, *Phys. Rev. B* **13**, 5188 (1976).
- [56] T. Fukui, Y. Hatsugai, and H. Suzuki, Chern Numbers in Discretized Brillouin Zone: Efficient Method of Computing (Spin) Hall Conductances, *J. Phys. Soc. Jpn.* **74**, 1674 (2005).
- [57] S.-W. Kim, H.-J. Kim, S. Cheon, and T.-H. Kim, Circular Dichroism of Emergent Chiral Stacking Orders in Quasi-One-Dimensional Charge Density Waves, *Phys. Rev. Lett.* **128**, 046401 (2022).
- [58] S. Freund and S. Teufel, Peierls substitution for magnetic Bloch bands, *Anal. PDE* **9**, 773 (2016).
- [59] T. Ozawa and B. Mera, Relations between topology and the quantum metric for Chern insulators, *Phys. Rev. B* **104**, 045103 (2021).
- [60] G. Vignale and M. Rasolt, Current- and spin-density-functional theory for inhomogeneous electronic systems in strong magnetic fields, *Phys. Rev. B* **37**, 10685 (1988).